# Mutation in the key enzyme of sialic acid biosynthesis causes severe glomerular proteinuria and is rescued by *N*-acetylmannosamine

Belinda Galeano,[1,2] Riko Klootwijk,[1] Irini Manoli,[1] MaoSen Sun,[1] Carla Ciccone,[1] Daniel Darvish,[3] Matthew F. Starost,[4] Patricia M. Zerfas,[4] Victoria J. Hoffmann,[4] Shelley Hoogstraten-Miller,[5] Donna M. Krasnewich,[1] William A. Gahl,[1,6] and Marjan Huizing[1]

[1]Medical Genetics Branch, National Human Genome Research Institute, NIH, Bethesda, Maryland, USA. [2]Howard Hughes Medical Institute/NIH Research Scholars Program, Bethesda, Maryland, USA. [3]HIBM Research Group, Encino, California, USA. [4]Division of Veterinary Resources, [5]Office of Laboratory Animal Medicine, National Human Genome Research Institute, and [6]Office of Rare Diseases, Office of the Director, NIH, Bethesda, Maryland, USA.

**Mutations in the key enzyme of sialic acid biosynthesis, uridine diphospho–*N*-acetylglucosamine 2-epimerase/*N*-acetylmannosamine (ManNAc) kinase (GNE/MNK), result in hereditary inclusion body myopathy (HIBM), an adult-onset, progressive neuromuscular disorder. We created knockin mice harboring the M712T Gne/Mnk mutation. Homozygous mutant ($Gne^{M712T/M712T}$) mice did not survive beyond P3. At P2, significantly decreased Gne-epimerase activity was observed in $Gne^{M712T/M712T}$ muscle, but no myopathic features were apparent. Rather, homozygous mutant mice had glomerular hematuria, proteinuria, and podocytopathy. Renal findings included segmental splitting of the glomerular basement membrane, effacement of podocyte foot processes, and reduced sialylation of the major podocyte sialoprotein, podocalyxin. ManNAc administration yielded survival beyond P3 in 43% of the $Gne^{M712T/M712T}$ pups. Survivors exhibited improved renal histology, increased sialylation of podocalyxin, and increased Gne/Mnk protein expression and Gne-epimerase activities. These findings establish this $Gne^{M712T/M712T}$ knockin mouse as what we believe to be the first genetic model of podocyte injury and segmental glomerular basement membrane splitting due to hyposialylation. The results also support evaluation of ManNAc as a treatment not only for HIBM but also for renal disorders involving proteinuria and hematuria due to podocytopathy and/or segmental splitting of the glomerular basement membrane.**

## Introduction

The *GNE* gene encodes the bifunctional enzyme uridine diphospho–*N*-acetylglucosamine (UDP-GlcNAc) 2-epimerase/*N*-acetylmannosamine (ManNAc) kinase (GNE/MNK), which is ubiquitously expressed and catalyzes the first 2 committed, rate-limiting steps in the biosynthesis of 5-*N*-acetylneuraminic acid (Neu5Ac, also known as sialic acid) (Figure 1) (1–3). The epimerase enzyme is feedback inhibited by the downstream product, cytidine monophosphate Neu5Ac. Neu5Ac is the most abundant mammalian sialic acid and is found as the terminal sugar on glycoconjugates, where it functions in cellular interactions and signaling (2–4).

Mutations in the *GNE* gene result in the autosomal recessive neuromuscular disorder hereditary inclusion body myopathy (HIBM) (OMIM 600737). HIBM is characterized by adult-onset, slowly progressive muscle weakness and atrophy (5, 6). Serum creatine kinase levels are normal to slightly elevated and electromyograms show either a myopathic or a neuropathic pattern. Histologically, muscle fibers degenerate and develop filamentous nuclear inclusions and cytoplasmic rimmed vacuoles (5, 6). No therapy currently exists for HIBM. A *GNE* founder mutation (M712T) was described in Persian-Jewish HIBM families (7), and numerous other *GNE* mutations exist worldwide (8–10). HIBM-associated *GNE* mutations result in reduced activity of both GNE and MNK (11, 12), which is thought to be responsible for reduced sialic acid production.

The pathologic mechanism of muscle fiber degeneration in HIBM remains unknown (12–18). However, evidence suggests that decreased availability of sialic acid in muscle causes hyposialylation of muscle glycoproteins, whether involving glycans in general (12, 13), O-linked glycans in particular (14), polysialic acid on neural cell adhesion molecules (PSA-NCAM) (15, 16), or specific *O*-mannosylated glycosyl residues on α-dystroglycan (18).

One hypothesis is that provision of free sialic acid could increase glycoprotein sialylation in HIBM muscle and ameliorate the myopathic symptoms. Sialic acid might be administered in its free form, bound as glycoconjugates, or as its precursor ManNAc, which is uncharged and crosses membranes readily. ManNAc is also situated in the sialic acid biosynthesis pathway after the regulated, rate-limiting GNE step (Figure 1), so its metabolism is not subject to feedback inhibition. Residual MNK activity in HIBM patients, or ancillary kinases such as GlcNAc kinase (19), might convert ManNAc into ManNAc-6-phosphate for subsequent synthesis of sialic acid. In fact, hyposialylated, *Gne*-deficient mouse

**Nonstandard abbreviations used:** *Col4A3*, collagen type IV α3; GBM, glomerular basement membrane; GlcNAc, *N*-acetylglucosamine; GNE, UDP-GlcNAc 2-epimerase; HIBM, hereditary inclusion body myopathy; ManNAc, *N*-acetylmannosamine; MNK, ManNAc kinase; PSA-NCAM, polysialic acid on neural cell adhesion molecules; UDP, uridine diphospho.

**Conflict of interest:** The authors have declared that no conflict of interest exists.

**Citation for this article:** *J. Clin. Invest.* **117**:1585–1594 (2007). doi:10.1172/JCI30954.

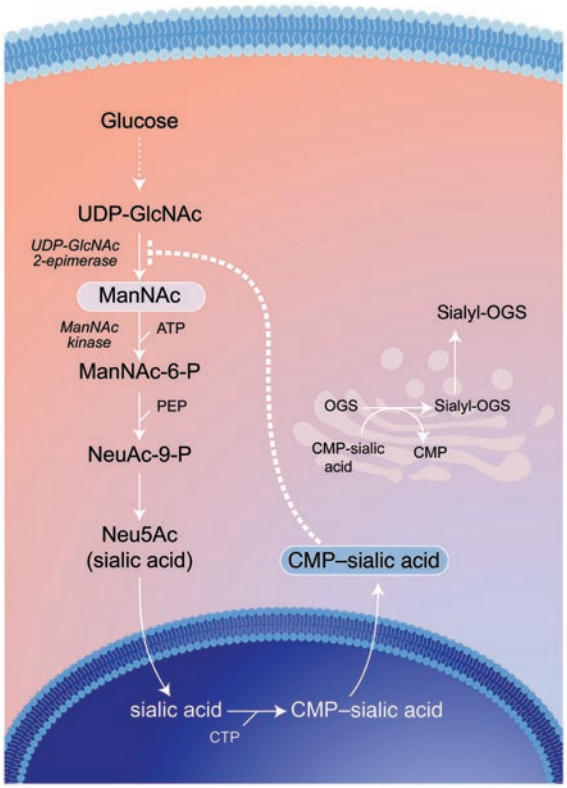


**Figure 1**
Intracellular sialic acid metabolism. Cytosolic glucose is converted in several steps into UDP-GlcNAc, which serves as substrate for the bifunctional, rate-limiting, committed enzyme of sialic acid biosynthesis, GNE/MNK. The GNE catalytic activity (EC 5.1.3.14) epimerizes UDP-GlcNAc to ManNAc, followed by the phosphorylation of ManNAc to ManNAc-6-phosphate (MaNAc-6-P) by the MNK kinase catalytic domain (EC 2.7.1.60). ManNAc-6-P is then further converted into Neu5Ac (sialic acid), which is activated into cytidine monophosphate–sialic acid (CMP–sialic acid) in the nucleus. CMP–sialic acid can subsequently be utilized in the Golgi complex as a substrate for the biosynthesis of sialyl-oligosaccharides by sialyltransferases. Cytosolic CMP–sialic acid displays strong feedback inhibition (dotted line) of GNE enzymatic activity by binding to its allosteric site (1), thereby contributing to the tight regulation of intracellular sialic acid biosynthesis. Even more complexity is added to this pathway by the presence of ancillary kinases, such as GlcNAc kinase (NAGK; EC 2.7.1.59) with high intrinsic MNK activity (19), which can also convert ManNAc to ManNAc-6-P. CTP, cytidine triphosphate; PEP, phosphoenolpyruvate; OGS, oligosaccharides.

embryonic stem cells became resialylated after their growth medium was supplemented with ManNAc (16). Furthermore, incubation of cultured cells with "unnatural" ManNAc derivatives, i.e., *N*-levulinoylmannosamine (ManLev) or *N*-azidoacetylmannosamine (ManNAz), resulted in incorporation of the downstream sialic acid analogs (SiaLev or SiaNAz) into cell surface glycoconjugates (20). Importantly, oral supplementation of $^{14}$C-ManNAc to healthy rats showed incorporation of the $^{14}$C label into several tissues, including kidney and muscle (21).

In order to test sialic acid replacement therapies in an animal model of HIBM, we created a gene-targeted knockin mouse homozygous for the M712T *Gne* mutation ($Gne^{M712T/M712T}$). Here, we extensively characterize this mouse, which died within 72 hours after birth, lacking a muscle phenotype. Homozygous mice had severe glomerular hematuria and podocytopathy, including effacement of the podocyte foot processes and segmental splitting of the glomerular basement membrane (GBM), likely due to hyposialylation of specific membrane glycoproteins. Unexpectedly, these knockin mice provide a novel animal model of podocytopathy and/or segmental splitting of the GBM, demonstrating the significance of sialic acid synthesis in kidney development and function. Administration of ManNAc to pregnant mice had a remarkably salutary effect on the survival and renal disease of homozygous pups and was associated with increased enzymatic activity of GNE, increased sialylation of kidney podocalyxin, and improved morphology of the podocyte foot processes and GBM integrity. This study supports consideration of ManNAc not only as a treatment for HIBM but also for treatment of kidney disorders characterized by segmental splitting of the GBM and/or podocytopathy due to disturbed polyanions on podocyte membranes.

## Results

*Generation of $Gne^{M712T/M712T}$ knockin mice*. A murine targeting vector for homologous recombination in C57BL/6J embryonic stem cells was constructed to include the M712T *Gne* mutation (Figure 2A). The neomycin phosphotransferase and thymidine kinase genes were introduced into the vector as positive and negative selection markers, respectively (Figure 2A). Additional *Lox*P (flanking exon 12 and *neo*) and flippase recombinase target sites (flanking *neo*) were inserted, allowing for potential future conditional transgenic models (22). The entire vector was sequence verified. Genotyping of the mice was performed by PCR amplification and digestion with the restriction endonuclease NlaIII (Figure 2B). Tissues of homozygous mutant $Gne^{M712T/M712T}$ and wild-type $Gne^{+/+}$ mice showed comparable Gne RNA transcript levels by real-time quantitative PCR. Furthermore, NlaIII digestion of amplified cDNA demonstrated homozygous insertion of the M712T mutation in RNA of $Gne^{M712T/M712T}$ mice (Figure 2C).

*Early postnatal lethality*. Initial matings of heterozygous mice ($Gne^{M712T/+}$) yielded 101 offspring from which only 1 $Gne^{M712T/M712T}$ animal survived beyond P21. The remaining $Gne^{M712T/M712T}$ offspring died at P1–P3 (Figure 2D). However, subsequent genotyping of 35 embryos at days E17–E19 showed 26% $Gne^{+/+}$, 43% $Gne^{M712T/+}$, and 31% $Gne^{M712T/M712T}$, reflecting a Mendelian distribution, statistically confirmed by goodness-of-fit testing ($\chi^2 = 0.94$, $P = 0.62$) (Figure 2D). At E17–E19, the embryos displayed normal exteriors, normal head and body sizes, and pink skin, which indicated good circulatory and respiratory function. By P2, however, $Gne^{M712T/M712T}$ mice were smaller than control littermates (Figure 2E), weighing 70%–100% of control littermates. The $Gne^{M712T/M712T}$ mouse stomachs contained milk, although a prominent milkspot was not always visible. All $Gne^{M712T/M712T}$ mice except 1 died by P3 and had increased urinary protein. In contrast, $Gne^{M712T/+}$ mice appeared unaffected.

*Histological analyses*. Tissues of $Gne^{M712T/M712T}$ mice and their littermates were examined between age P2 and P3. No abnormalities were identified in skeletal muscle (Supplemental Figure 1A; supplemental material available online with this article; doi:10.1172/JCI30954DS1), heart, or liver (data not shown). Moreover, immunohistochemical staining with antibodies against laminin (Supplemental Figure 1B) and dystrophin (Supplemental Figure 1C) failed to show differences between muscle sections of $Gne^{M712T/M712T}$ mice and their wild-type littermates.

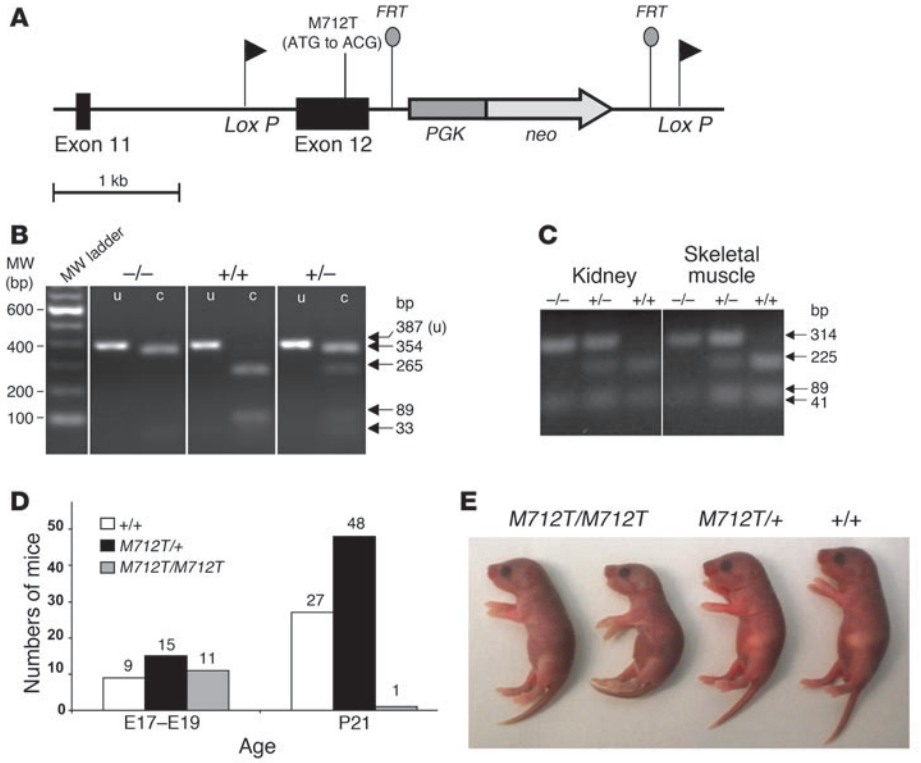


**Figure 2**

Generation and identification of *Gne*$^{M712T/M712T}$ knockin mice. (**A**) Resultant murine *Gne* (*Uea1*) genomic locus, exons 11 and 12, after homologous recombination with the sequence-verified targeting vector. The M712T mutation was created in exon 12, and a *neo* cassette (under the PGK promoter) flanked by *flippase recombinase target* (*FRT*) sites was inserted. *LoxP* sites were inserted before exon 12 and after the PGK-*neo* gene. (**B**) Genotyping of mutant mice. A PCR-amplified 387-bp fragment of genomic DNA across the M712T (ATG to ACG) mutation was digested by the NlaIII restriction endonuclease into 265-bp, 89-bp, and 33-bp fragments in a wild-type allele (+) and into 354-bp and 33-bp fragments in a mutant M712T allele (–). c, cut; MW, molecular weight; u, uncut. (**C**) RT-PCR of kidney and skeletal muscle RNA. RNA was reverse transcribed and PCR-amplified using primers covering exons 11 and 12 (355 bp). Digestion by NlaIII cut the wild-type allele (+) into 225-bp, 89-bp, and 41-bp fragments and the mutant M712T allele (–) into 314-bp and 41-bp fragments. Digestion confirmed the exclusive presence of the mutant M712T allele in *Gne*$^{M712T/M712T}$ (–/–) tissues. (**D**) Numbers of mice at E17–E19 and P21. At P21, genotyping of 76 mice from 13 litters (9 *Gne*$^{M712T/+}$ matings) identified only 1 *Gne*$^{M712T/M712T}$ offspring. Subsequent genotyping of 35 E17–E19 embryos from 4 *Gne*$^{M712T/+}$ mice yielded a Mendelian distribution of genotypes. (**E**) At P2, *Gne*$^{M712T/M712T}$ pups were smaller than their heterozygous (*Gne*$^{M712T/+}$) and wild-type (*Gne*$^{+/+}$) littermates and lacked a prominent milkspot.

Ultrastructural analyses of the glomeruli at age P2 revealed that, compared with the slender, well-shaped glomerular foot processes of wild-type mice (Figure 4A), the podocyte foot process membranes of *Gne*$^{M712T/M712T}$ mice were flattened and largely fused, with only a few wide foot processes remaining (Figure 4B). Filtration slits were reduced in number and showed formation of tight junction–like structures (Figure 4B). In addition, the GBM showed segmental splitting of the lamina densa (Figure 4B). The size and shape of endothelial cells lining the GBM, as well as glomerular mesangial cells, appeared ultrastructurally intact.

To support these ultrastructural findings, additional analyses were performed using markers for specific glomerular compartments. The podocyte-specific markers podocin and podocalyxin (23, 24) were tested by immunoblotting kidney extracts of all genotypes. While podocin showed no difference in expression across all genotypes (at age P1) (data not shown), podocalyxin, the major sialoglycoprotein of the podocyte apical membrane (23, 24), demonstrated dramatically decreased sialylation (Figure 5E, upper gel). Expression levels of GBM markers laminin-1 (Figure 5C) and laminin β1 (Supplemental Figure 2A) were unchanged in *Gne*$^{M712T/M712T}$ kidneys, as were RNA levels of collagen type IV α3 (*Col4A3*), an integral GBM component (Supplemental Figure 2B) (25–27). Immunoblotting with desmin and vascular SMA, antibodies to mesangial cell markers (28), showed similar expression levels across all genotypes (Supplemental Figure 2A). In addition, real-time quantitative PCR analysis of the endothelial cell marker *CD31/Pecam-1* (29) revealed no difference in RNA expression levels across genotypes at P1 (Supplemental Figure 2B).

At age P2, kidneys of *Gne*$^{M712T/M712T}$ mice showed petechial hemorrhages by gross examination, but were normal in size and shape compared with kidneys of *Gne*$^{+/+}$ and *Gne*$^{M712T/+}$ littermates (Figure 3A). Histological analyses revealed cystic tubular dilatation (Figure 3B). High-magnification views of *Gne*$^{M712T/M712T}$ kidneys showed red blood cell infiltrates in the proximal and distal convoluted tubules and the collecting ducts (Figure 3C). The glomeruli of *Gne*$^{M712T/M712T}$ mice contained red blood cell infiltrates in Bowman space (Figure 3D). Of 100 glomeruli scored in each group, 64% ± 6% were affected in *Gne*$^{M712T/M712T}$ mice ($n = 4$) compared with 2% ± 1% in *Gne*$^{M712T/+}$ mice ($n = 3$) and 4% ± 4.5% in *Gne*$^{+/+}$ mice ($n = 4$). Immunohistochemical analysis demonstrated localization of Gne/Mnk antibodies to kidney glomeruli (Figure 3E). Examination of *Gne*$^{M712T/M712T}$ kidneys at E18 showed no histological differences compared with wild-type or heterozygous littermates (data not shown).

Serum metabolite studies on the only *Gne*$^{M712T/M712T}$ mouse that survived past weaning demonstrated elevated blood urea nitrogen levels (39 ± 10 mg/dl in *Gne*$^{M712T/M712T}$ mouse versus 21 ± 2 mg/dl in *Gne*$^{+/+}$ mice) and increased urinary protein (>500 mg/dl protein), which indicated renal disease. All other serum metabolites tested, including creatinine and creatine kinase, were within the normal ranges (Supplemental Figure 3C). This male *Gne*$^{M712T/M712T}$ survivor was euthanized at age 8.5 months. Histologic analysis revealed no structural abnormalities in the forelimb or hindlimb. However, severe bilateral hydronephrosis and changes consistent with glomerulopathy were found in the kidneys (Supplemental Figure 3, A and B).

*Rescue by ManNAc feeding.* ManNAc, added to the drinking water at a concentration of 1 mg/ml (~0.2 g/kg/day) during matings of

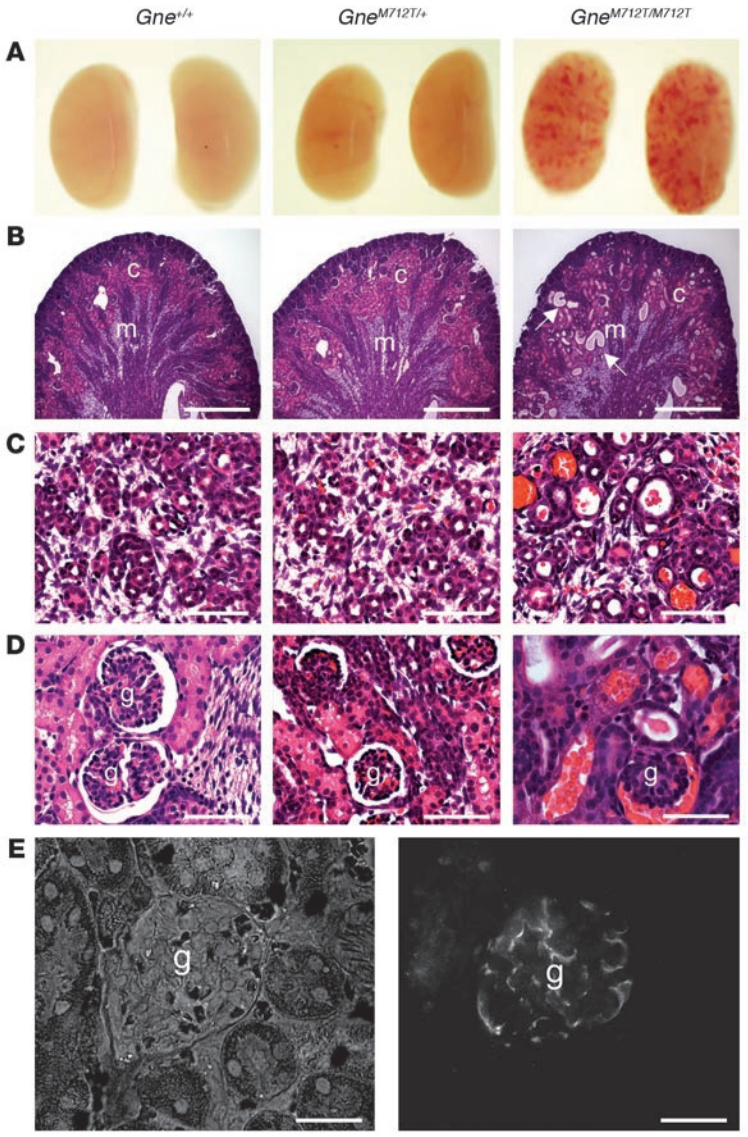


**Figure 3**
Histological kidney analyses. (**A**) Gross kidney pathology. Kidneys of *Gne*$^{M712T/M712T}$ mice showed hemorrhages but were normal in size and shape compared with kidneys of wild-type (*Gne*$^{+/+}$) and heterozygous (*Gne*$^{M712T/+}$) littermates. (**B**) Representative H&E-stained sections of renal cortex (c) and medulla (m) showing tubular dilatations in *Gne*$^{M712T/M712T}$ mice (arrows). Scale bars: 1,000 μm. (**C**) High magnification of collecting ducts, renal tubules, and urinary space, filled with rbc in *Gne*$^{M712T/M712T}$ mice. Scale bars: 100 μm. (**D**) High magnification of glomeruli (g) with rbc infiltrated into the Bowman space in *Gne*$^{M712T/M712T}$ mice. Scale bars: 100 μm. (**E**) Representative normal glomerulus (DICII filter, left panel) demonstrates abundance of Gne/Mnk protein inside the glomerular space upon immunolabeling with Gne/Mnk antibodies (FITC filter, right panel). Scale bars: 50 μm.

*Gne*$^{M712T/+}$ mice, yielded no surviving homozygous *Gne*$^{M712T/M712T}$ mice beyond age P3 from among 51 offspring (Figure 6A). However, at 5 mg ManNAc/ml (~1.0 g/kg/d), among 102 total newborns, 12 *Gne*$^{M712T/M712T}$ pups survived beyond P3, a significantly greater number compared with the 1 survivor in the untreated group (2-tailed Fisher's exact test, $P = 0.01$) (Figure 6A). ManNAc at the administered dose (~1.0 g/kg/d) was well tolerated by the mice, and no side effects were attributed to the treatment throughout the study. Surviving *Gne*$^{M712T/M712T}$ mice remained smaller than their wild-type littermates, weighing 70%–100%. At age P6, ManNAc treated *Gne*$^{M712T/M712T}$ mice exhibited no abnormalities in liver, heart, or skeletal muscle tissues (data not shown). Their kidneys demonstrated significant histological improvement (Figure 6, B–D) compared with *Gne*$^{M712T/M712T}$ mice examined at age P2 (Figure 3, B–D). Upon ManNAc treatment, there were fewer cystic tubular dilatations in the cortex and medulla (Figure 6B) and reduced red blood cell infiltrates in the tubules and the Bowman space (Figure 6, C and D). Ultrastructural analysis at age P19 showed less fusion and flattening of the podocyte foot processes including a greater number of open slit diaphragms and an improvement in the "finger shaping" of the foot processes (Figure 4, C and D). The overall integrity of the GBM was also significantly improved, although occasional segmental splitting of the lamina densa was still apparent (Figure 4, C and D).

The nursing females continued to receive ManNAc treatment until the pups were weaned (P21). Of the 12 *Gne*$^{M712T/M712T}$ mice that survived past P3, 9 died between P6 and P12. One *Gne*$^{M712T/M712T}$ mouse was sacrificed at age P19 for ultrastructural analysis. Two *Gne*$^{M712T/M712T}$ mice survived past P21, when ManNAc supplementation was ceased. These 2 mice continued to grow without receiving additional ManNAc but remained smaller than their littermates (Figure 6E). At 3.5 months of age, 1 *Gne*$^{M712T/M712T}$ survivor was sacrificed because of hydrocephalus and malocclusion. Similar events occurred in some untreated mice at different ages and were found not to be related to treatment or the disease. Skeletal muscle histology of this mouse revealed no structural or inflammatory abnormalities, but the kidneys showed mild red blood cell infiltrations in the urinary space and the tubules. The 1 surviving *Gne*$^{M712T/M712T}$ mouse is currently 6 months old and has no obvious myopathic features.

*Biochemical analyses following ManNAc feeding.* Gne enzymatic activity was measured in muscle and kidney at age P2. Skeletal muscle of *Gne*$^{M712T/M712T}$ mice showed 19.4% ± 7.5% of the Gne activity of the *Gne*$^{+/+}$ mice ($n = 4$, $P = 0.02$) (Figure 6F). Similar decreases in Gne activities were measured in *Gne*$^{M712T/M712T}$ kidney extracts (10% of mean *Gne*$^{+/+}$ kidney epimerase activities). Upon ManNAc treatment, Gne activities in *Gne*$^{+/+}$ muscle ($n = 3$) increased to 114% ± 19.7% ($P = 0.2$), while *Gne*$^{M712T/M712T}$ muscle activity ($n = 7$) increased from 19.4% ± 7.5% to 31% ± 8.4% of untreated *Gne*$^{+/+}$ mean values of muscle Gne activity ($P = 0.05$) (Figure 6F).

Immunoblots of muscle and kidney extracts labeled with anti-Gne/Mnk antibodies demonstrated 38.5% ± 27%, ($n = 4$) Gne/Mnk protein in *Gne*$^{M712T/M712T}$ muscle and 32.1% ± 7%, ($n = 3$) in *Gne*$^{M712T/M712T}$ kidney tissues when compared with *Gne*$^{+/+}$ littermates. This improved upon ManNAc treatment of *Gne*$^{M712T/M712T}$ mice to 68.8% ± 20%, ($n = 4$) in muscle and to 62.2% ± 9.7%, ($n = 4$) in kidney tissues ($P = 0.12$ and $P = 0.006$ for muscle and kidney values respectively, relative to β-actin) (Figure 5, A and B). Immunoblots stained with antibodies against laminin-1, an integral component of the GBM (25–27), showed similar patterns across genotypes before and after treatment (Figure 5C).

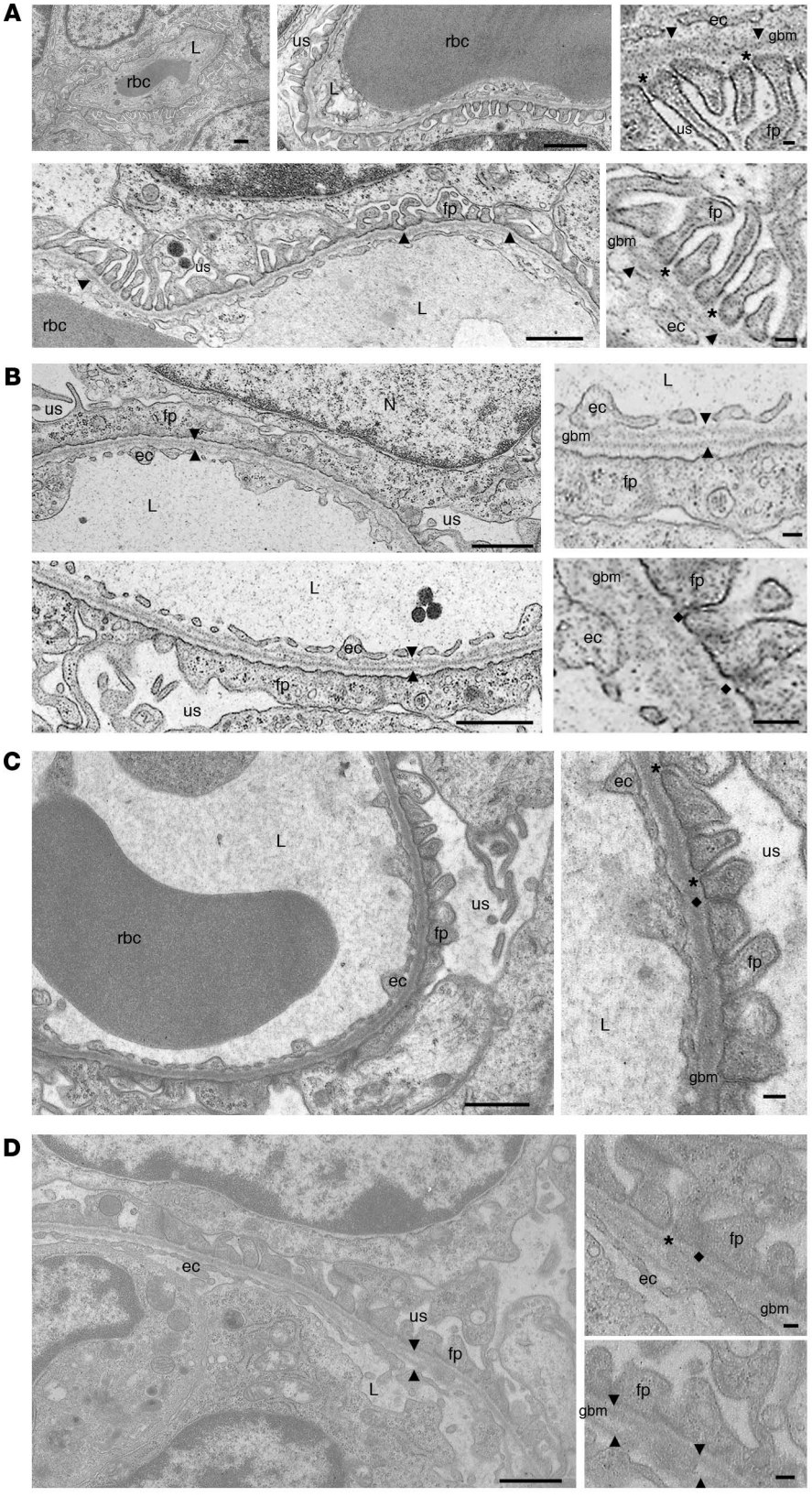


**Figure 4**
Transmission electron microscopy of mouse kidneys. (**A**) Representative cross-sections of glomerular capillaries in the juxtamedullar zone of a wild-type mouse (age P2). Enlarged insets (right panels) show detailed endothelial cells (ec), GBM (arrowheads), and foot processes (fp) of the glomerular epithelial cells (podocytes) with well formed, open filtration slits (asterisks). (**B**) Representative juxtamedullary glomerular capillaries of a *Gne*$^{M712T/M712T}$ mouse (age P2, littermate of the wild-type mouse shown in **A**), indicating segmental splitting of the lamina densa of the GBM (arrowheads) as well as dramatically flattened and fused podocyte foot processes lining the GBM. The filtration slits are sparse and irregular in shape and position. Insets (right panels) show fused foot process membranes and formation of abnormal tight junction-like structures at the filtration slits (diamonds). (**C** and **D**) Representative glomerular capillaries of a *Gne*$^{M712T/M712T}$ mouse following ManNAc treatment (age P19). The integrity of the GBM as well as the formation of podocyte foot processes and the number of filtration slits were all improved when compared with the untreated *Gne*$^{M712T/M712T}$ mouse in **B**. Some filtration slits were open, while others still formed tight junctions. The GBM showed occasional small stretches of areas where splitting was apparent (arrowheads). L, capillary lumen; N, nucleus; us, urinary space. Scale bars: 1 μm.

We then studied the degree of sialylation of 2 heavily sialylated marker proteins, PSA-NCAM and podocalyxin. PSA-NCAM is a major sialoprotein expressed in neonatal brains (30), where its expression is regulated by the intracellular concentration of sialic acid (31). Our results showed that the expression of PSA-NCAM varied within and between genotypes, yet *Gne*$^{M712T/M712T}$ brains at P2 showed up to 80% decreased PSA-NCAM expression compared with that in *Gne*$^{+/+}$ mice (Figure 5D, upper gel). A 2%–28% increase compared with *Gne*$^{M712T/M712T}$ untreated mice following ManNAc treatment was observed ($n = 14$ before treatment and $n = 10$ after treatment, $P = 0.08$) (Figure 5D, lower gel). The expression of PSA-NCAM in normal muscle and kidney at P2 was low, and no change upon treatment in these tissues could be confirmed (data not shown).

In addition, the significantly decreased sialylation status of podocalyxin in untreated *Gne*$^{M712T/M712T}$ kidneys (Figure 5E, lower gel) markedly improved upon ManNAc treatment (Figure 5E, upper gel).

## Discussion

Research into HIBM lacks an understanding of basic pathogenic mechanisms, an animal model, and an effective therapy. We took a first step toward addressing these issues by creating a Gne gene–targeted knockin mouse mimicking the M712T mutation of Persian-Jewish HIBM patients. With the exception of 1

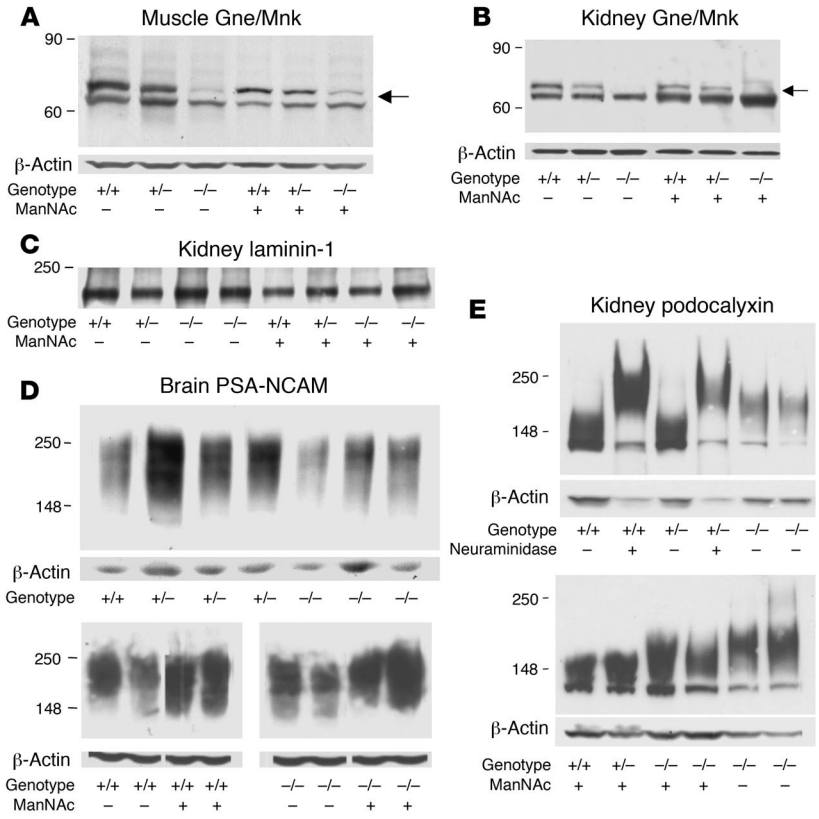


**Figure 5**
Immunoblotting of muscle, kidney, and brain extracts of knockin mice. Immunoblots of muscle (**A**) and kidney (**B**) extracts showed decreased Gne/Mnk protein expression (upper band, arrows, 79 kDa) in homozygous mutant $Gne^{M712T/M712T}$ (–/–) mice compared with heterozygous (+/–) and wild-type (+/+) littermates (normalized to β-actin). Gne/Mnk protein expression increased upon ManNAc feeding in $Gne^{M712T/M712T}$ (–/–) tissues when compared with untreated tissues. (**C**) Immunoblots of kidney extracts labeled with laminin-1 antibodies. No difference in laminin-1 intensity was detected ($n = 6$; $P = 0.65$) between $Gne^{+/+}$ (+/+) and $Gne^{M712T/M712T}$ (–/–) littermates without or with ManNAc treatment. (**D**) Representative immunoblots of brain extracts labeled with PSA-NCAM antibodies. Upon ManNAc treatment, the intensity of the PSA-NCAM signals, reflecting sialylation status, increased by 2% to 28% in treated $Gne^{M712T/M712T}$ (–/–) brain ($n = 14$) when compared with untreated brain ($n = 10$). (**E**) Immunoblots of kidney extracts (age P2) labeled with antibodies against podocalyxin (~140–150 kDa). Top: Following desialylation of $Gne^{+/+}$ (+/+), $Gne^{M712T/+}$ (+/–), or $Gne^{M712T/M712T}$ (–/–) kidney extracts by neuraminidase (lanes 2 and 4), podocalyxin migrated more slowly (~160–180 kDa) (24) than untreated samples (lanes 1 and 3). $Gne^{M712T/M712T}$ (–/–) kidney extracts (lanes 5 and 6) contained desialylated podocalyxin. Bottom: Sialylation of podocalyxin at P6 in $Gne^{M712T/M712T}$ (–/–) mice changed significantly after ManNAc treatment (lanes 3 and 4).

male, homozygous mutated ($Gne^{M712T/M712T}$) mice did not survive past age P3 (Figure 2D) and showed no muscle pathology at age P2 (Supplemental Figure 1). The lack of early myopathic features recapitulates the human HIBM phenotype. In both cases, the muscle pathology may occur late or be attenuated because a modicum of sialic acid is provided through the actions of residual Gne/Mnk enzymatic activities (11, 12) (Figure 5, A and B, and Figure 6F) supplemented by ancillary enzymes such as GlcNAc kinase (NAGK) (19) and generic sugar kinases. Eventually, the $Gne^{M712T/M712T}$ mice may develop myopathic features, if they can be maintained well past weaning. Even very young mutant mice exhibited hyposialylation of PSA-NCAM (i.e., in brain) (Figure 5D), previously reported in skeletal muscle of HIBM patients (15) and in embryonic stem cells of *Gne* knockout mice (16).

Remarkably, the $Gne^{M712T/M712T}$ mice clearly differed from HIBM patients in their manifestation of an apparently lethal renal phenotype. The mice exhibited early glomerular disease, with red blood cell infiltrates (Figure 3, A–D), effacement of podocyte foot processes, and segmental splitting of the lamina densa of the GBM (Figure 4B), resulting in death within 72 hours after birth. In our group of human HIBM patients, we have no indication of renal abnormalities. Laboratory findings were all within normal ranges, including levels of blood urea nitrogen, creatinine, and urine 24-hour protein and glucose (32). We know of no reports of abnormal urinary laboratory values in patients with HIBM.

We showed that Gne/Mnk localized to mouse kidney glomeruli (Figure 3E), a site with high sialic acid concentrations (33, 34). Humans and mice differ in the relative importance of sialic acid to the kidney, and they certainly differ in the type of sialic acid present. Most mammalian species utilize the sialic acid Neu5Gc (*N*-glycolylneuraminic acid), but humans have lost the ability to synthesize Neu5Gc (35) and rely on Neu5Ac as their main sialic acid. Protein glycosylation patterns also vary; the glomerular sialoprotein podocalyxin itself differs widely among species in the contingent of *O*- and *N*-linked glycosylation sites in its extracellular aminoterminal region (36). Future studies, such as employing the Cre-Lox system to create conditional Gne knockouts (22), might shed light on these issues.

The morphologic abnormalities of podocytes and GBM in the $Gne^{M712T/M712T}$ mouse represent surprising and important findings. Podocytes are glomerular epithelial cells that provide the architecture of the glomerular filtration apparatus, including interdigitating foot processes, slit diaphragms, and the intercellular urinary spaces (23, 37, 38). The negatively charged sialic acid residues on glycoproteins such as α-dystroglycan, α3β1-integrin, and podocalyxin are essential for the function of podocyte foot processes (24, 33, 34) and they act as antiadhesion molecules, assisting in maintaining an open urinary space, filtration slits, and Bowman space. Disruption of podocalyxin or neutralization of its negative charge resulted in dissociation of podocalyxin from the actin cytoskeleton and led to foot process effacement (39). Indeed, we demonstrated the presence of hyposialylated podocalyxin in $Gne^{M712T/M712T}$ mouse kidney extracts (Figure 5E) along with effacement of foot processes and malformed filtration slits (Figure 4B). Some forms of glomerular disease (such as minimal change nephrosis; ref. 40) exhibit hyposialylation of foot process glycoproteins, with subsequent deformation of podocyte membranes and proteinuria (33, 34, 37, 38, 41–43).

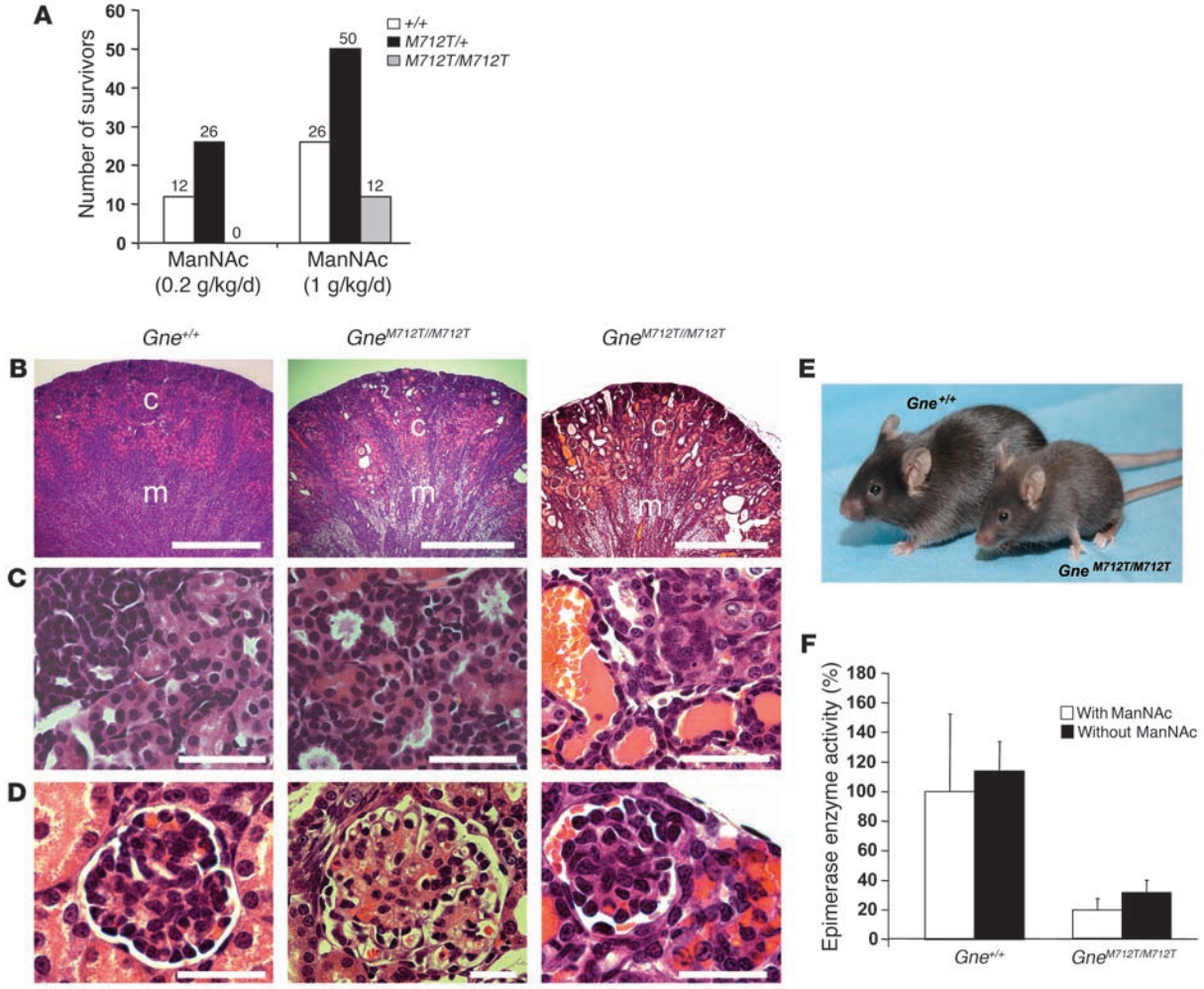


**Figure 6**

Biochemistry and renal histology of knockin mice following ManNAc treatment. (**A**) Numbers of mice surviving past age P3 after ManNAc administration in the drinking water of $Gne^{M712T/+}$ mice. Six $Gne^{M712T/+}$ mice received 1 mg/ml (~0.2 g/kg/d) ManNAc; 7 total litters were scored; 13 pups died at age P1–P3. Seven $Gne^{M712T/+}$ mice received 5 mg/ml (~1 g/kg/d) ManNAc; 13 total litters were scored; 14 homozygous mutant pups died at age P1–P3. The percentage of survivors of each genotype is indicated. (**B**–**D**) Representative H&E-stained kidney sections showing renal cortex and medulla (**B**); collecting ducts, renal tubules, and urinary space (**C**); and glomeruli (**D**) following ManNAc feeding at age P6. Wild-type ($Gne^{+/+}$) kidneys showed normal histology. $Gne^{M712T/M712T}$ kidneys showed a range from very mild (middle panel) to moderately severe (right panel) rbc infiltrations, but in all cases less severe than in untreated $Gne^{M712T/M712T}$ mice at age P2 (Figure 3, E–G). Scale bars: 500 μm (**B**), 100 μm (**C** and **D**). (**E**) Two ManNAc-treated (~1 g/kg/d) 6-week-old male littermates. Surviving homozygous mutant mice ($Gne^{M712T/M712T}$) were smaller than their wild-type littermates. (**F**) Gne/Mnk epimerase enzymatic activities in skeletal muscle. Administration of ManNAc increased the activity in wild-type muscle from 100% to 114% ± 19.7% ($n$ = 3; $P$ = 0.2) and increased the activity in homozygous mutant ($Gne^{M712T/M712T}$) muscle from 19.4% ± 7.5% to 31% ± 8.4% ($n$ = 7; $P$ = 0.05).

Effacement of podocyte foot processes has also been reported for mice lacking podocalyxin (44), nephrin (45), or the giant protocadherin mFAT1 (46), all leading to proteinuria and death within 72 hours of birth. Other laboratory models have been created to study the phenomenon of effacement of foot processes due to general hyposialylation; these include sialidase inoculation in mice, resulting in hyposialylation of podocalyxin (41), supplementation studies with purine aminonucleoside (47), and perfusion of a polycation protamine sulfate (48). To our knowledge, our $Gne^{M712T/M712T}$ knockin mouse is the first *genetic* model demonstrating podocyte flattening and fusion events due to hyposialylation, resulting in proteinuria.

Interestingly, our mutant mice also displayed hematuria, a feature that can be attributed to structural GBM defects (Figure 4B), which allow red blood cells to gain access to Bowman space, as occurs in thin GBM disease (49). The segmental GBM splitting in our knockin mice might have resulted from defects in expression levels or charge of specific proteins. In contrast to the findings on podocalyxin (Figure 5E), testing of other compartment-specific markers, some of which are affected in renal GBM disorders, did not reveal any defects in expression levels in $Gne^{M712T/M712T}$ kidneys. These included GBM markers laminin-1, laminin β1, and *Col4A3* (dysregulated in Alport disease) (25–27, 50) (Figure 5C and Supplemental Figure 2) and the podocyte marker podocin (data not

shown) (38). Advanced investigations are required to further elucidate the glomerular phenotype in our $Gne^{M712T/M712T}$ mice. Nevertheless, the severe renal findings of podocytopathy and GBM splitting are likely responsible for the proteinuria, hematuria, and early death in our mice.

Although the exact cause of neonatal lethality in the $Gne^{M712T/M712T}$ mice remains elusive, their rescue by ManNAc suggests that sialic acid deficiency was involved. Outcome parameters included survival (Figure 6A), improved renal histology (Figure 6, B–D), including a markedly improved integrity of the GBM (Figure 4, C and D), less flattened and fused podocyte foot processes (Figure 4, C and D), increased sialylation of renal podocalyxin (Figure 5E), and increased sialylation of brain PSA-NCAM (Figure 5D), all likely related to augmented production of sialic acid. Since ManNAc supplementation increased skeletal muscle Gne epimerase activity (Figure 6F) and Gne/Mnk protein expression (Figure 5, A and B), we suggest that ManNAc improved catalytic activity by stabilizing the normal and the mutant enzymes. Similar stabilization effects on other proteins have been demonstrated using natural or artificial ligands or chaperones (51, 52). The effects of ManNAc on *Gne* mutations other than M712T deserve further investigation.

$Gne^{M712T/M712T}$ mice can be used to determine the optimal sialic acid repletion therapy for HIBM. Our knockin mice may eventually develop myopathic features similar to the adult-onset myopathy of HIBM patients; treatment could then be geared toward preventing the specific muscle disease. We recently observed a transient but significant improvement in the muscle strength of HIBM patients who received intravenous immune globulin G, and it is hypothesized that this effect is mediated through the large sialic acid content provided by the immune globulin (32). Other sources of sialic acid may also be reasonable candidates for treating HIBM, especially if they show efficacy in the appropriate mouse model.

In conclusion, we consider the uncharged, physiological monosaccharide ManNAc a promising therapeutic option for HIBM, particularly for patients harboring the M712T *GNE* mutation. In addition, ManNAc may have therapeutic potential for some podocytopathies. Candidate disorders include minimal change nephrosis (40), focal and segmental glomerulosclerosis (53), membranous glomerulonephritis (54), and other forms of unexplained idiopathic nephrotic syndrome (55). The $Gne^{M712T/M712T}$ mice unexpectedly provide a unique opportunity to study basic mechanisms and targeted therapies of podocyte injury and/or GBM splitting, for which appropriate model systems are sparse (23, 38, 56, 57). This is especially true for disorders involving proteinuria and/or hematuria for which the etiology is unknown and may be related to changes in charge (sialylation) of GBM components. Increased survival of the M712T *Gne* knockin mice could serve as an absolute outcome parameter for potential therapeutic interventions, and resolution of renal disease could provide a graded measure of response.

## Methods

*$Gne^{M712T/M712T}$ mice*. $Gne^{M712T/M712T}$ knockin mice were generated by targeting the M712T (ATG to ACG) mutation of exon 12 of the murine *Gne* gene (*Gne*, *Uae1*, GenBank NM_015828) (Figure 2A). The mutant mice were maintained in the C57BL/6J background. Animals were housed in an Association for Assessment and Accreditation of Laboratory Animal Care International–accredited specific pathogen–free facility in accordance with the *Guide for the care and use of laboratory animals* (NIH publication no. 85-23. Revised 1985). Cages were ventilated in a temperature- and light-controlled environment (22°C, 30%–70% humidity, 12-hour light/12-hour dark cycle). The mice were fed irradiated chow (Prolab 5P75 Isopro 3000; PMI Nutrition International) and sterile water ad libitum. All euthanasia was performed by $CO_2$ inhalation followed by cervical dislocation. For Mendelian distribution studies, 4 pregnant mice at E17–E19 were euthanized, and embryos were retrieved by cesarean section and euthanized by decapitation. All mouse procedures were performed in accordance with protocol G04-3 and were approved by the Institutional Animal Care and Use Committee of the National Human Genome Research Institute.

*Molecular analysis*. Mouse genotyping was performed on tail genomic DNA or cDNA isolated from kidney or skeletal muscle using standard protocols. Total RNA was isolated from murine tissues using the TRIzol reagent (Invitrogen), and cDNA was prepared using the SuperScript III system (Invitrogen). PCR amplifications were performed across the M712T mutation with genomic DNA as template, using the primer set 5′-AGCACTTCCTGGAGTTTGATG-3′ and 5′-ATTTGCCTTCGCAGAAACACTTGA-3′ (Figure 2B) or with cDNA as template (Figure 2C), using the primer set 5′-GCCCAGAGCATCTTACGAAC-3′ and 5′-GGGTCCCCTGGAGCTTGG-3′ and PuReTaq Ready-To-Go PCR beads (GE HealthCare), using standard PCR conditions. PCR fragments were digested with NlaIII at 37°C to verify the mutation status (Figure 2, B and C). Quantitative real-time PCR was performed on RNA isolated from kidney and skeletal muscle, utilizing Assays-On-Demand (Applied Biosystems) for *Gne* (Assay ID mm00607939_s1), *Pecam-1* (Assay ID mm00476702_m1), *Col4A3* (Assay ID mm01269206_g1), and β-*actin* (Assay ID mm00450174_s1) on an ABI PRISM 7900 HT Sequence Detection System (Applied Biosystems).

*Clinical chemistry screen*. Retroorbital blood samples (100–150 μl) from age-matched, weaned male mice weighing at least 15 grams were obtained bimonthly after pretreatment with a topical anesthetic (0.5% tetracaine HCl; Bausch & Lomb Pharmaceuticals). Samples were allowed to clot (30 minutes at room temperature) in MicroPrep centrifuge tubes (IRIS International Inc.), after which the serum was separated by centrifugation at 1,500 *g* for 10 minutes and stored at –80°C until analysis. Clinical chemistry screens were performed at the Department of Laboratory Medicine at the NIH and included monitoring of creatinine, blood urea nitrogen, albumin, total protein, uric acid, alkaline phosphatase, alanine aminotransferase, aspartate aminotransferase, amylase, creatine kinase, and lactate dehydrogenase. In addition, reagent strips for protein urinalysis were used to assess proteinuria (Chemstrip 2GP; Roche Diagnostics).

*Antibodies*. A rabbit polyclonal antibody was custom prepared against a Gne/Mnk peptide comprising amino acids 588–607 (EAYASGMALQREAKKLHDED), coupled to keyhole limpet hemocyanine, and affinity purified against the corresponding antigenic peptide (Covance). The following additional primary antibodies were commercially obtained: dystrophin (catalog no. ab15277; Abcam); laminin-1 (catalog no. L9393; Sigma-Aldrich); podocalyxin (catalog no. PODX15-A; Alpha Diagnostic International); podocin (catalog no. P0372; Sigma-Aldrich); laminin β1 (catalog no. MAB1928; Millipore); desmin (catalog no. 1466-1; Epitomics); VSMA (α-SMA) (SPM332; GeneTex Inc.); PSA-NCAM (catalog no. MAB5324; Millipore); and β-actin (catalog no. AAN01; Cytoskeleton).

*Mouse histology*. Mouse tissues were collected, formalin fixed (10%) and paraffin embedded. Tissue sections (5 μm) were stained with H&E following standard procedures (American Histolabs) or subjected to immunohistochemistry with a variety of primary antibodies (Gne/Mnk, dystrophin, and laminin-1. Formalin-fixed tissues were deparaffinized in HistoClear II (National Diagnostics) and dehydrated in a series of ethanol solutions. Antigen retrieval was performed for sections that were to be stained with antibodies against Gne/Mnk (by boiling 5 minutes in citric acid–based solution; Vector Laboratories) and against dystrophin (by boiling in 1 mM EDTA according the manufacturer's protocol; AbCam). The

sections were blocked (2% BSA, 10% donkey serum, and 0.1% Triton X-100 in PBS) and incubated with primary antibodies (Gne/Mnk 1:50; laminin 1:25; dystrophin 1:50) overnight at 4°C, followed by incubation with the secondary antibody, Alexa Fluor 488–conjugated donkey anti-rabbit (1:500 in blocking solution) (Invitrogen). The sections were mounted in VECTASHIELD Mounting Medium (Vector Laboratories) and viewed and digitally imaged with a Zeiss Axiovert 200M microscope (Zeiss).

*Western blotting*. Mouse tissues (age P2) were extracted, homogenized in CelLytic buffer consisting of a mild detergent, bicine buffer, and 150 mM NaCl (Sigma-Aldrich) supplemented with protease inhibitors (Complete Mini; Roche Applied Science). The lysates were sonicated and cleared by centrifugation (1,000 *g* for 10 minutes), and the resulting supernatants were assayed for protein (BCA Protein Assay; Pierce Biotechnology). For the neuraminidase enzymatic treatments (Figure 5E), protein homogenates (25 μg) were incubated for 30 min at 37°C with 1 mU/μg of neuraminidase (catalog no. N6514; Sigma-Aldrich). Equal amounts of protein (25–50 μg) were electrophoresed on 4%–12% Tris-Glycine gels (Novex; Invitrogen), and electroblotted onto 0.45 μm Hybond ECL nitrocellulose membranes (GE HealthCare). The membranes were blocked (10% fat-free milk) and incubated with primary antibodies discussed above in "Antibodies" followed by HRP-conjugated secondary antibodies (GE HealthCare). Results were visualized with ECL (ECL Western Blotting Detection Reagents; GE HealthCare) and exposure to CL-XPosure Film (Pierce Biotechnology). Densitometry was performed on the digital images obtained with a Kodak Image Station 2000R and Kodak 1D 3.6 software (PerkinElmer). The protein levels were normalized to those of β-actin to correct for differences in protein loading and/or transfer.

*Electron microscopy*. Kidney samples were fixed overnight at 4°C in 2% glutaraldehyde in 0.1 M cacodylate buffer (pH 7.4) and washed with cacodylate buffer. After fixation with 1% $OsO_4$ for 2 hours and a second wash with 0.1 M cacodylate buffer, the tissues were serially dehydrated in ethanol and embedded in Eponate 12 resin (Ted Pella). Thin sections (~80 nm) were obtained using a Leica Ultracut UCT Ultramicrotome (Leica Microsystems), placed onto 400 mesh copper grids, and stained with saturated uranyl acetate in 50% methanol followed by lead citrate. The grids were viewed with a Philips 410 transmission electron microscope (FEI Company) at 80 kV, and images were recorded on Electronic Image Film SO-163 (Kodak).

*ManNAc administration*. Breeding pairs of 6-week-old $Gne^{M712T/+}$ mice were divided into 3 groups. Group I consisted of 9 $Gne^{M712T/+}$ breeding pairs, who were administered untreated sterilized tap water. Group II consisted of 1 breeding pair of $Gne^{+/+}$ mice (wild-type control) and 6 $Gne^{M712T/+}$ breeding pairs, who were administered water containing 1 mg/ml (~0.2 g/kg/day) ManNAc (Sigma-Aldrich). That dose was selected based on previous evidence of the safety of ManNAc (administered at a single dose of 0.142 g/kg/day) in a study performed in humans (21). Group III consisted of 1 $Gne^{+/+}$ breeding pair and 7 $Gne^{M712T/+}$ breeding pairs, who were administered water supplemented with 5 mg/ml (~1.0 g/kg/day) ManNAc. Water was changed twice weekly. Nursing females continued to be supplied with ManNAc. All mice were weaned from ManNAc at 21 days. Selected whole litters were euthanized at age P2, P6, and P19 for histological, genetic, biochemical, or ultrastructural analysis.

*Gne enzymatic assays*. Mouse kidney and skeletal muscle (quadriceps) tissues were homogenized and subjected to the Gne-epimerase enzymatic assay as previously described (11, 58). This assay was based on incubation with radiolabeled substrate UDP-[$^3$H]GlcNac (catalog no. ART 1136; American Radiolabeled Chemicals Inc.) and detection of radiolabeled product [$^3$H]ManNAc upon separation of oligosaccharides by high-pH anion-exchange chromatography with pulsed amperometric detection (BioLC carbohydrate analyzer and CarboPac PA-100 Column; Dionex) (32).

*Statistics*. Differences between data groups were evaluated for significance using the 2-tailed Student's *t* test of unpaired data. For Mendelian distribution analysis, a goodness-of-fit ($\chi^2$) test was performed, while for comparisons of survival between treated and untreated mice of all genotypes ($Gne^{+/+}$, $Gne^{M712T/+}$, and $Gne^{M712T/M712T}$), a 2-tailed Fisher's exact test using a 2 × 3 table was employed. All data are presented as the mean ± SD. A *P* value less than 0.05 was considered statistically significant.

## Acknowledgments

The authors thank Theresa Calhoun, Gene Elliott, Emily Gottlieb, Wesley Bond, and Shahrouz Naiem for their skilled assistance with mouse maintenance. We greatly appreciate the expert evaluation of histological data by Michael Eckhaus. This study was supported by the Intramural Research Program of the National Human Genome Research Institute.

Received for publication November 14, 2006, and accepted in revised form March 27, 2007.

Address correspondence to: Marjan Huizing, Medical Genetics Branch, National Human Genome Research Institute, National Institutes of Health, 10 Center Drive, Building 10, Room 10C103, Bethesda, Maryland 20892-1851, USA. Phone: (301) 402-2797; Fax: (301) 480-7825; E-mail: mhuizing@mail.nih.gov.

MaoSen Sun's present address is: Institute for Translational Medicine and Therapeutics and Cardiovascular Institute, University of Pennsylvania School of Medicine, Philadelphia, Pennsylvania, USA.

Belinda Galeano and Riko Klootwijk contributed equally to this work.

1. Hinderlich, S., Stasche, R., Zeitler, R., and Reutter, W. 1997. A bifunctional enzyme catalyzes the first two steps in N-acetylneuraminic acid biosynthesis of rat liver. Purification and characterization of UDP-N-acetylglucosamine 2-epimerase/N-acetylmannosamine kinase. *J. Biol. Chem.* **272**:24313–24318.
2. Keppler, O.T., et al. 1999. UDP-GlcNAc 2-epimerase: a regulator of cell surface sialylation. *Science.* **284**:1372–1376.
3. Huizing, M. 2005. Disease mechanisms associated with mutations of the GNE gene. *Drug Discovery Today Disease Mechanisms.* **2**:519–527.
4. Varki, A. 1997. Sialic acids as ligands in recognition phenomena. *FASEB J.* **11**:248–255.
5. Griggs, R.C., et al. 1995. Inclusion body myositis and myopathies. *Ann. Neurol.* **38**:705–713.
6. Sivakumar, K., and Dalakas, M.C. 1996. The spectrum of familial inclusion body myopathies in 13 families and a description of a quadriceps-sparing phenotype in non-Iranian Jews. *Neurology.* **47**:977–984.
7. Eisenberg, I., et al. 2001. The UDP-N-acetylglucosamine 2-epimerase/N-acetylmannosamine kinase gene is mutated in recessive hereditary inclusion body myopathy. *Nat. Genet.* **29**:83–87.
8. Nishino, I., et al. 2002. Distal myopathy with rimmed vacuoles is allelic to hereditary inclusion body myopathy. *Neurology.* **59**:1689–1693.
9. Eisenberg, I., et al. 2003. Mutations spectrum of GNE in hereditary inclusion body myopathy sparing the quadriceps. *Hum. Mutat.* **21**:99.
10. Broccolini, A., et al. 2004. Novel GNE mutations in Italian families with autosomal recessive hereditary inclusion-body myopathy. *Hum. Mutat.* **23**:632.
11. Sparks, S.E., et al. 2005. Use of a cell-free system to determine UDP-N-acetylglucosamine 2-epimerase and N-acetylmannosamine kinase activities in human hereditary inclusion body myopathy. *Glycobiology.* **15**:1102–1110.
12. Noguchi, S., et al. 2004. Reduction of UDP-N-acetylglucosamine 2-epimerase/N-acetylmannosamine kinase activity and sialylation in distal myopathy with rimmed vacuoles. *J. Biol. Chem.* **279**:11402–11407.
13. Saito, F., et al. 2004. A Japanese patient with distal myopathy with rimmed vacuoles: missense mutations in the epimerase domain of the UDP-N-acetylglucosamine 2-epimerase/N-acetylmannosamine kinase (GNE) gene accompanied by hyposialylation of skeletal muscle glycoproteins. *Neuromuscul. Disord.* **14**:158–161.
14. Tajima, Y., et al. 2005. Distal myopathy with rimmed vacuoles: impaired O-glycan formation in muscular glycoproteins. *Am. J. Pathol.* **166**:1121–1130.
15. Ricci, E., et al. 2006. NCAM is hyposialylated in

hereditary inclusion body myopathy due to GNE mutations. *Neurology.* **66**:755–758.
16. Schwarzkopf, M., et al. 2002. Sialylation is essential for early development in mice. *Proc. Natl. Acad. Sci. U. S. A.* **99**:5267–5270.
17. Hinderlich, S., et al. 2004. The homozygous M712T mutation of UDP-N-acetylglucosamine 2-epimerase/N-acetylmannosamine kinase results in reduced enzyme activities but not in altered overall cellular sialylation in hereditary inclusion body myopathy. *FEBS Lett.* **566**:105–109.
18. Huizing, M., et al. 2004. Hypoglycosylation of alpha-dystroglycan in patients with hereditary IBM due to GNE mutations. *Mol. Genet. Metab.* **81**:196–202.
19. Hinderlich, S., et al. 1998. Purification and characterization of N-acetylglucosamine kinase from rat liver--comparison with UDP-N-acetylglucosamine 2-epimerase/N-acetylmannosamine kinase. *Eur. J. Biochem.* **252**:133–139.
20. Charter, N.W., Mahal, L.K., Koshland, D.E., Jr., and Bertozzi, C.R. 2000. Biosynthetic incorporation of unnatural sialic acids into polysialic acid on neural cells. *Glycobiology.* **10**:1049–1056.
21. Amir, S.M., Barker, S.A., Butt, W.R., Crooke, A.C., and Davies, A.G. 1966. Administration of N-acetyl-D-mannosamine to mammals. *Nature.* **211**:976–977.
22. Nagy, A. 2000. Cre recombinase: the universal reagent for genome tailoring. *Genesis.* **26**:99–109.
23. Pavenstadt, H., Kriz, W., and Kretzler, M. 2003. Cell biology of the glomerular podocyte. *Physiol. Rev.* **83**:253–307.
24. Dekan, G., Gabel, C., and Farquhar, M.G. 1991. Sulfate contributes to the negative charge of podocalyxin, the major sialoglycoprotein of the glomerular filtration slits. *Proc. Natl. Acad. Sci. U. S. A.* **88**:5398–5402.
25. Hansen, K., and Abrass, C.K. 1999. Role of laminin isoforms in glomerular structure. *Pathobiology.* **67**:84–91.
26. Abrahamson, D.R., Prettyman, A.C., Robert, B., and St. John, P.L. 2003. Laminin-1 reexpression in Alport mouse glomerular basement membranes. *Kidney Int.* **63**:826–834.
27. Abrahamson, D.R. 1985. Origin of the glomerular basement membrane visualized after in vivo labeling of laminin in newborn rat kidneys. *J. Cell Biol.* **100**:1988–2000.
28. Ichimura, K., Kurihara, H., and Sakai, T. 2006. Involvement of mesangial cells expressing alpha-smooth muscle actin during restorative glomerular remodeling in Thy-1.1 nephritis. *J. Histochem. Cytochem.* **54**:1291–1301.
29. Ricono, J.M., et al. 2003. Morphological insights into the origin of glomerular endothelial and mesangial cells and their precursors. *J. Histochem. Cytochem.* **51**:141–150.
30. Galuska, S.P., et al. 2006. Polysialic acid profiles of mice expressing variant allelic combinations of the polysialyltransferases ST8SiaII and ST8SiaIV. *J. Biol. Chem.* **281**:31605–31615.
31. Bork, K., Reutter, W., Gerardy-Schahn, R., and Horstkorte, R. 2005. The intracellular concentration of sialic acid regulates the polysialylation of the neural cell adhesion molecule. *FEBS Lett.* **579**:5079–5083.
32. Sparks, S., et al. 2007. Intravenous immune globulin in hereditary inclusion body myopathy: a pilot study. *BMC Neurol.* **7**:3.
33. Charest, P.M., and Roth, J. 1985. Localization of sialic acid in kidney glomeruli: regionalization in the podocyte plasma membrane and loss in experimental nephrosis. *Proc. Natl. Acad. Sci. U. S. A.* **82**:8508–8512.
34. Andrews, P.M. 1979. Glomerular epithelial alterations resulting from sialic acid surface coat removal. *Kidney Int.* **15**:376–385.
35. Chou, H.H., et al. 1998. A mutation in human CMP-sialic acid hydroxylase occurred after the Homo-Pan divergence. *Proc. Natl. Acad. Sci. U. S. A.* **95**:11751–11756.
36. Kershaw, D.B., et al. 1997. Molecular cloning and characterization of human podocalyxin-like protein. Orthologous relationship to rabbit PCLP1 and rat podocalyxin. *J. Biol. Chem.* **272**:15708–15714.
37. Vogtlander, N.P., et al. 2005. Localization of alpha-dystroglycan on the podocyte: from top to toe. *J. Histochem. Cytochem.* **53**:1345–1353.
38. Tryggvason, K., Patrakka, J., and Wartiovaara, J. 2006. Hereditary proteinuria syndromes and mechanisms of proteinuria. *N. Engl. J. Med.* **354**:1387–1401.
39. Takeda, T., McQuistan, T., Orlando, R.A., and Farquhar, M.G. 2001. Loss of glomerular foot processes is associated with uncoupling of podocalyxin from the actin cytoskeleton. *J. Clin. Invest.* **108**:289–301. doi:10.1172/JCI200112539.
40. Saha, T.C., and Singh, H. 2006. Minimal change disease: a review. *South. Med. J.* **99**:1264–1270.
41. Gelberg, H., Healy, L., Whiteley, H., Miller, L.A., and Vimr, E. 1996. In vivo enzymatic removal of alpha 2—>6-linked sialic acid from the glomerular filtration barrier results in podocyte charge alteration and glomerular injury. *Lab. Invest.* **74**:907–920.
42. Raats, C.J., et al. 2000. Expression of agrin, dystroglycan, and utrophin in normal renal tissue and in experimental glomerulopathies. *Am. J. Pathol.* **156**:1749–1765.
43. Vogtlander, N.P., et al. 2006. Reactive oxygen species deglycosilate glomerular alpha-dystroglycan. *Kidney Int.* **69**:1526–1534.
44. Doyonnas, R., et al. 2001. Anuria, omphalocele, and perinatal lethality in mice lacking the CD34-related protein podocalyxin. *J. Exp. Med.* **194**:13–27.
45. Putaala, H., Soininen, R., Kilpelainen, P., Wartiovaara, J., and Tryggvason, K. 2001. The murine nephrin gene is specifically expressed in kidney, brain and pancreas: inactivation of the gene leads to massive proteinuria and neonatal death. *Hum. Mol. Genet.* **10**:1–8.
46. Ciani, L., Patel, A., Allen, N.D., and Ffrench-Constant, C. 2003. Mice lacking the giant protocadherin mFAT1 exhibit renal slit junction abnormalities and a partially penetrant cyclopia and anophthalmia phenotype. *Mol. Cell. Biol.* **23**:3575–3582.
47. Caulfield, J.P., Reid, J.J., and Farquhar, M.G. 1976. Alterations of the glomerular epithelium in acute aminonucleoside nephrosis. Evidence for formation of occluding junctions and epithelial cell detachment. *Lab. Invest.* **34**:43–59.
48. Seiler, M.W., Rennke, H.G., Venkatachalam, M.A., and Cotran, R.S. 1977. Pathogenesis of polycation-induced alterations ("fusion") of glomerular epithelium. *Lab. Invest.* **36**:48–61.
49. Collar, J.E., Ladva, S., Cairns, T.D., and Cattell, V. 2001. Red cell traverse through thin glomerular basement membranes. *Kidney Int.* **59**:2069–2072.
50. Hudson, B.G., Tryggvason, K., Sundaramoorthy, M., and Neilson, E.G. 2003. Alport's syndrome, Goodpasture's syndrome, and type IV collagen. *N. Engl. J. Med.* **348**:2543–2556.
51. Welch, W.J., and Howard, M. 2000. Antagonists to the rescue. *J. Clin. Invest.* **105**:853–854.
52. Chaudhuri, T.K., and Paul, S. 2006. Protein-misfolding diseases and chaperone-based therapeutic approaches. *FEBS J.* **273**:1331–1349.
53. Daskalakis, N., and Winn, M.P. 2006. Focal and segmental glomerulosclerosis. *Cell. Mol. Life Sci.* **63**:2506–2511.
54. Ronco, P., and Debiec, H. 2006. New insights into the pathogenesis of membranous glomerulonephritis. *Curr. Opin. Nephrol. Hypertens.* **15**:258–263.
55. Vats, A.N. 2005. Genetics of idiopathic nephrotic syndrome. *Indian J. Pediatr.* **72**:777–783.
56. Durvasula, R.V., and Shankland, S.J. 2006. Podocyte injury and targeting therapy: an update. *Curr. Opin. Nephrol. Hypertens.* **15**:1–7.
57. Shankland, S.J. 2006. The podocyte's response to injury: role in proteinuria and glomerulosclerosis. *Kidney Int.* **69**:2131–2147.
58. Weiss, P., Tietze, F., Gahl, W.A., Seppala, R., and Ashwell, G. 1989. Identification of the metabolic defect in sialuria. *J. Biol. Chem.* **264**:17635–17636.